Organic Electronics 15 (2014) 2148–2157

Contents lists available at ScienceDirect

Organic Electronics

journal homepage: www.elsevier.com/locate/orgel

Tetrasubstituted-pyrene derivatives for electroluminescent application

Rossatorn Muangpaisal [a,b,c], Ming-Chi Ho [b,d], Tai-Hsiang Huang [b], Chih-Hsin Chen [b], Jiun-Yi Shen [b], Jen-Shyang Ni [b], Jiann T. Lin [b,*], Tung-Huei Ke [e], Li-Yin Chen [e], Chung-Chih Wu [e,*], Chiitang Tsai [d,*]

[a] *Taiwan International Graduate Program, Taiwan*
[b] *Institute Chemistry, Academia Sinica, Taipei 11529, Taiwan*
[c] *Department of Chemistry, National Tsing Hua University, 101 Section 2 Kuang-Fu Road, Hsinchu 30031,Taiwan*
[d] *Department of Chemistry, Chinese Culture University, Taipei 111, Taiwan*
[e] *Department of Electrical Engineering, Graduate Institute of Electro-optical Engineering and Graduate Institute of Electronics Engineering, National Taiwan University, Taipei 106, Taiwan*

ARTICLE INFO

Article history:
Received 21 February 2014
Received in revised form 21 April 2014
Accepted 2 June 2014
Available online 21 June 2014

Keywords:
Pyrene
Star-shaped materials
Organic light-emitting diode
Ambipolar transport

ABSTRACT

Tetrasubstituted-pyrenes containing peripheral diarylamines (**1**–**4**) or fluorenes (**5**–**6**) have been synthesized. These compounds are highly fluorescent and possess high morphological stability and thermal stability. Compounds containing peripheral arylamines (**1**–**3**) can be used as the hole-transport and green-emitting materials for two-layered electroluminescent devices. Compounds with peripheral fluorenes (**5**–**6**) are efficient blue emitters and exhibit ambipolar carrier-transport characteristics with high electron mobilities (10^{-3}–10^{-2} cm^2/V s) and high hole mobilities (>10^{-3} cm^2/V s). Non-doped blue-emitting devices with promising electroluminescent performance (i.e., high efficiency and narrow/saturated emission) can be achieved using fluorene–substituted pyrenes as either the hole-transport/emitting layer or the electron-transport/emitting layer in the two-layered devices.

1. Introduction

Two decades after Kodak's [1] and Cambridge's [2] seminal work on organic electroluminescence (EL), organic light-emitting diodes (OLEDs) have become widely used in practical appliances such as car stereos, mobile phones, and digital cameras. In OLEDs, balanced electron and hole mobilities are extremely important in order to achieve good EL performance. Through proper choice of carrier-transport and emitting materials, and engineering of device structures, better confinement of charge recombination can generally be achieved in a multilayer device. Moreover, longevity of EL devices is also highly demanded for commercial applications. Therefore, the durability, e.g., thermal and morphological stability of deposited organic films, cannot be overlooked. Unlike polymeric materials which can easily form films via the spin-coating technique, films of small molecules normally are vacuum-deposited. Consequently, the compounds must be able to tolerate the deposition temperature, which frequently exceeds 250 °C. Amorphous compounds possessing high glass transition temperatures (T_g) are highly desired as crystallization can be avoided and film morphology can be retained at elevated temperatures during device operation [3–6].

Molecules possessing a non-planar structure and different conformers have a great tendency to form amorphous glasses [5]. Among these, star-shaped π-conjugated molecules allowing incorporation of several bulky and

---

* Corresponding authors. Tel.: +886 2 27898522.
E-mail addresses: jtlin@chem.sinica.edu.tw (J.T. Lin), chungwu@cc.ee.ntu.edu.tw (C.-C. Wu), tsaictom@faculty.pccu.edu.tw (C. Tsai).

http://dx.doi.org/10.1016/j.orgel.2014.06.003
1566-1199/

rigid substituents are of particular interest. Previously we developed several series of star-shaped compounds which readily formed glasses once isolated. These high T_g materials were successfully used to fabricate efficient electroluminescent (EL) devices [7,8]. In our continuation of developing high T_g materials for EL applications, we selected 1,3,6,8-tetrabromo-pyrene as the building block for new star-shaped compounds based on the following reasons: (1) according to our previous studies and other literature reports, incorporation of the pyrenyl unit was beneficial in raising the thermal stability of the compounds [9,10], (2) tetraphenylpyrene was reported to be strongly emissive [11] and (3) pyrenyl unit can be readily functionalized and its emission color can be tuned [12,13]. Compounds containing pyrenyl units have found useful applications in liquid crystals [14,15] and field-effect transistors [16,17]. Besides, the pyrenyl unit and its excimer was found useful in sensing [18–20]. However, formation of excimers normally quenches the fluorescence and deteriorate the performance of EL devices [21]. Star-shaped pyrenyl derivatives obtained by replacing four bromine atoms of 1,3,6,8-tetrabromopyrene with appropriate peripheral substituents are expected to encapsulate the pyrenyl moiety and prevent the formation of excimers. Moreover, incorporation of carrier-transporting peripheral substituents is possible. There have been reports on using 1,3,6,8-substituted pyrenyl derivatives as the light emitting materials in OLEDs [19]. Liu et al. developed pyrene derivatives containing four peripheral oligofluorenes of varied chain lengths. Single-layered OLED based on these materials exhibited a luminance efficiency of 1.28 cd A^{-1} with CIE coordinates at (0.19, 0.32) and 1.75 cd A^{-1} with CIE coordinates at (0.20, 0.32) for bifluorene and tris(fluorene) derivatives, respectively [22]. Sonar et al. developed pyrene-based compounds capable of emitting various colors by incorporation of different moieties. Among these, only the deep blue-emitting 1,3,6,8-tetrakis-(4-butoxyphenyl)pyrene was subjected to OLED fabrication, and high luminance efficiency of 2.56 cd A^{-1} with CIE coordinates at (0.15, 0.18) was achieved [23]. Recently, Thomas et al. reported blue to yellow light-emitting materials based on tetrasubstituted-pyrene core with acetylene unit as the linker to the peripheries, and these compounds exhibited red-shifted emission compared to the monosubstituted derivatives. However, these materials need to be doped in a host for OLEDs, possibly due to lack of amorphous morphology [24].

Herein, we report light-emitting 1,3,6,8-substituted pyrene derivatives possessing high quantum efficiency and carrier mobility. EL devices fabricated from these star-shaped materials will be also presented.

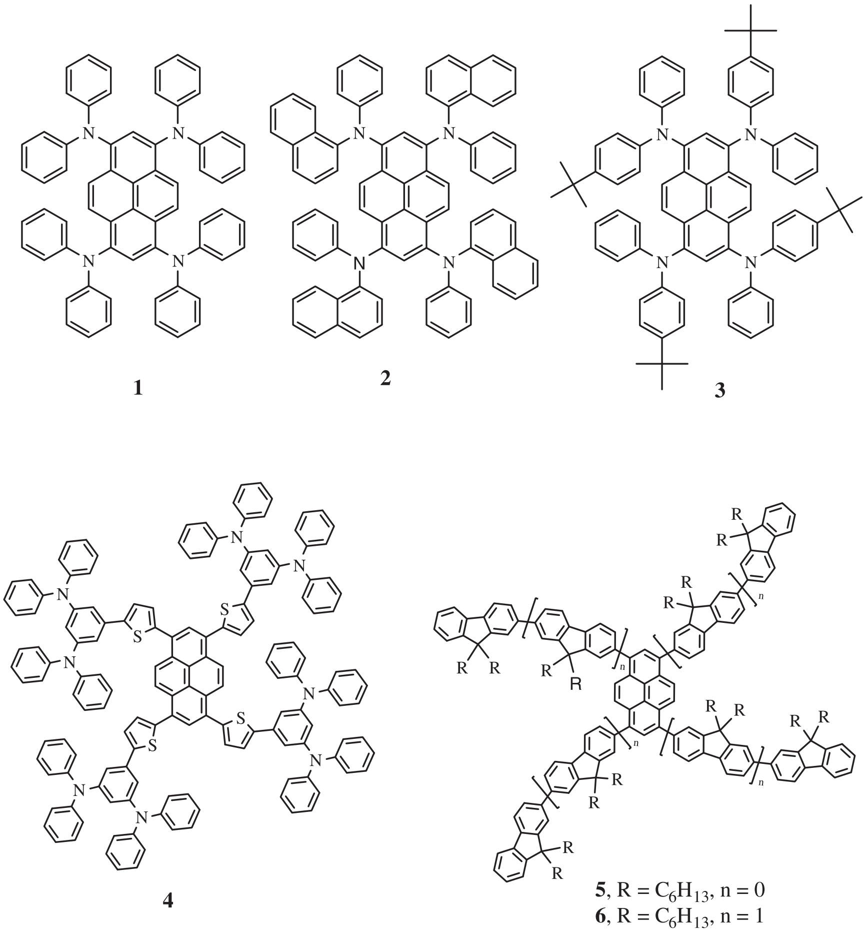

Chart 1. Structure of compounds **1–6**.

2. Experimental section

2.1. Materials and methods

All reactions and manipulations were carried out under N_2 with the use of standard inert atmosphere and Schlenk techniques. Solvents were dried by standard procedures. All column chromatography was performed with the use of silica gel (230–400 mesh, Macherey–Nagel GmbH & Co.) as the stationary phase in a column 30 cm in length and 4.0 cm in diameter. The NMR spectra were recorded on Bruker AMX400 and AC300 spectrometers. Electronic absorption spectra were measured in dichloromethane using a Cary 50 Probe UV–visible spectrophotometer. Emission spectra were recorded by a Jasco FP-6500 fluorescence spectrometer. Luminescence quantum yields (Φ_f) were calculated using Coumarin 1 as primary standard ($\Phi_f = 0.99$ in ethyl acetate) [25]. Cyclic voltammetry experiments were performed with a CHI-621B electrochemical analyzer. All measurements were carried out at room temperature with a conventional three electrode configuration consisting of a platinum working electrode, an auxiliary electrodes and a non-aqueous Ag/$AgNO_3$ reference electrode. The $E_{1/2}$ values were determined as $1/2(E_p^a + E_p^c)$, where E_p^a and E_p^c are the anodic and cathodic peak potentials, respectively. The solvent in all experiments was CH_2Cl_2 and the supporting electrolyte was 0.1 M tetrabutylammonium hexafluorophosphate. DSC measurements were carried out using a Perkin Elmer 7 series thermal analyzer at a heating rate of 10 °C/min. TGA measurements were performed on a Perkin Elmer TGA7 thermal analyzer. FAB-mass spectra were collected on a JMS-700 double focusing mass spectrometer (JEOL, Tokyo, Japan) with a resolution of 8000 (5% valley definition). For FAB-mass spectra, the source accelerating voltage was operated at 10 kV with a Xe gun, using 3-nitrobenzyl alcohol as the matrix. Elementary analyses were performed on a Perkin-Elmer 2400 CHN analyzer.

2.2. Synthesis and characterization

1,3,6,8-Tetrabromopyrene was synthesized as reported in the literature [26]. Compounds octaphenylpyrene-1,3,6,8-tetraamine (**1**), tetra(naphthalen-1-yl)-tetraphenylpyrene-1,3,6,8-tetra-amine (**2**), and 1,3,6,8-tetrakis(4-*tert*-butylphenyl)-1,3,6,8-tetraphenyl-pyrene-1,3,6,8-tetraamine (**3**) were synthesized by similar procedures, and only the preparation of **1** will be described in detail.

2.2.1. Octaphenylpyrene-1,3,6,8-tetraamine (*1*)

To a flask containing a mixture of 1,3,6,8-tetrabromopyrene (0.52 g, 1.0 mmol), diphenylamine (0.74 g, 4.4 mmol), sodium *tert*-butoxide (0.51 g, 5.28 mmol) and Pd(dba)$_2$ (0.040 mmol) was added dry toluene (30 mL). After 30 min. P(^{t}Bu)$_3$ (1.2 mol%) was added and the solution mixture was heated to reflux and stirred for 24 h. After cooling, the solution was pumped dry and the residue was extracted with CH_2Cl_2/brine. The organic layer was dried over magnesium sulfate, then filtered and dried. After recrystallization from dichloromethane and hexane, the crude product was further purified by column chromatography using CH_2Cl_2/hexane (1:10 by v/v) as eluent to give **1** as a yellow powder (0.82 g, 92%). ^{1}H NMR (400 MHz, acetone-d_6): δ (ppm) 7.96 (s, 4 H, pyrene), 7.67 (s, 2 H, pyrene), 7.15 (t, $J = 8.64$ Hz, 16 H, *meta*-C_6H_5), 6.99 (d, $J = 8.67$ Hz, 16 H, *ortho*-C_6H_5), 6.89 (t, $J = 8.66$ Hz, 8 H, *para*-C_6H_5); MS (FAB): *m*/*z* 870.1 (M^+). Anal. Calcd for $C_{64}H_{46}N_4$: C, 88.25; H, 5.32; N, 6.43. Found: C, 87.97; H, 5.45; N, 6.41.

2.2.2. Tetra(naphthalen-1-yl)-tetraphenylpyrene-1,3,6,8-tetra-amine (*2*)

Yield: 52%. Yellow powder. ^{1}H NMR (400 MHz, acetone-d_6): δ (ppm) 7.90 (s, 4 H, pyrene), 7.84 (d, $J = 8.47$ Hz, 4 H, $C_{10}H_{11}$), 7.81 (d, 8.45 Hz, 4 H, $C_{10}H_{11}$), 7.37 (s, 2 H, pyrene), 7.60 (d, $J = 8.40$ Hz, 4 H, $C_{10}H_{11}$), 7.39 (t, $J = 8.42$ Hz, 4 H, $C_{10}H_{11}$), 7.23 (t, $J = 8.39$ Hz, 4 H, $C_{10}H_{11}$), 7.18 (t, $J = 8.40$ Hz, 4 H, $C_{10}H_{11}$), 7.00–6.96 (m, $J = 8.44$ Hz, 8 H, *meta*-C_6H_5), 6.81 (t, $J = 8.45$ Hz, 8 H, *para*-C_6H_5), 6.60 (d, $J = 8.47$ Hz, 8 H, *ortho*-C_6H_5); MS (FAB): *m*/*z* 1070.3 (M^+). Anal. Calcd for $C_{80}H_{54}N_4$: C, 89.69; H, 5.08; N, 5.23. Found: C, 89.10; H, 5.64; N, 5.18.

2.2.3. 1,3,6,8-Tetrakis(4-tert-butylphenyl)-1,3,6,8-tetraphenyl-pyrene-1,3,6,8-tetraamine (*3*)

Yield: 52%. Yellow powder. ^{1}H NMR (400 MHz, acetone-d_6): δ (ppm) 8.00 (s, 4 H, pyrene). 7.66 (s, 2 H, pyrene), 7.24 (d, $J = 7.04$ Hz, 8 H, C_6H_4), 7.17 (t, $J = 7.20$ Hz, 8 H, C_6H_5), 6.98 (m, 16 H, *meta*-C_6H_5 and meta-C_6H_4), 6.86 (t, $J = 7.26$ Hz, 4 H, C_6H_5), 1.23 (s, 36 H, CH_3); MS (FAB): *m*/*z* 1095.5 (M^+). Anal. Calcd for $C_{80}H_{78}N_4$: C, 87.71; H, 7.18; N, 5.11. Found: C, 87.93; H, 6.70; N, 5.19.

2.2.4. 5-(5-(1,3,6-Tris(5-(3,5-bis(diphenylamino)phenyl)thiophen-2-yl)pyren-8-yl)thio-phen-2-yl)-1,1,3,3-tetraphenylbenzene-1,3-diamine (*4*)

To the flask containing a mixture of 1,3,6,8-tetrabromopyrene (0.52 g, 1.0 mmol), 5-(5-(tributylstannyl)thiophen-2-yl)-1,1,3,3-tetraphenylbenzene-1,3-diamine (3.45 g, 4.4 mmol) and $PdCl_2(PPh_3)_2$ (22 mg, 0.030 mmol) was added DMF (5 mL), and the mixture was heated at 80 °C for 48 h. After cooling, MeOH was added and the precipitate formed was collected by filtration. the crude product was further purified by column chromatography using CH_2Cl_2/hexane (2:5 by v/v) as eluent to give the **4** as a pale yellow powder (1.76 g, 61%). ^{1}H NMR (400 MHz, acetone-d_6): δ (ppm) 8.41 (s, 4 H, pyrene), 8.07 (s, 2 H, pyrene), 7.23–7.17 (m, 40 H, *meta*-C_6H_5 and C_4SH_2), 7.11 (d, $J = 7.47$ Hz, 32 H, *ortho*-C_6H_5), 6.98–6.95 (m, 24 H, *para*-C_6H_5, C_6H_3), 6.75 (s, 4 H, C_6H_3); MS (FAB): *m*/*z* 2173.6 (M^+). Anal. Calcd for $C_{80}H_{78}N_4$: C, 84.02; H, 4.92; N, 5.16. Found: C, 83.63; H, 5.01; N, 5.05.

2.2.5. 1,3,6,8-Tetrakis(9,9-dihexyl-9H-fluoren-2-yl)pyrene (*5*)

To the flask containing a mixture of 9,9-dihexyl-9*H*-fluoren-2-ylboronic acid (7.93 g, 21.0 mmol), 1,3,6,8-tetrabromopyrene (2.11 g, 4.04 mmol), Na_2CO_3 (2 M in H_2O, 9.0 mL, 8.9 mmol), and $Pd(PPh_3)_4$ (0.49 g, 0.42 mmol) was added 70 mL of dry toluene. After the reaction mixture was refluxed for 24 h, the solvent was removed and the residue was extracted with CH_2Cl_2/brine. The organic layer was dried over magnesium sulfate, then filtered and dried.

The crude product was further purified by column chromatography using CH_2Cl_2/hexane (1:5 v/v) as eluent to give the **5** as a pale yellow powder (3.5 g, 57%). ^1H NMR (400 MHz, acetone-d_6): δ (ppm) 8.18 (s, 4 H, pyrene), 8.14 (s, 2 H, pyrene), 7.84 (d, J = 7.45 Hz, 4 H, C_6H_3), 7.66–7.65 (m, 8 H, C_6H_3), 7.73 (d, J = 7.41 Hz, 4 H, C_6H_4), 7.37–7.29 (m, 12 H, C_6H_4), 2.00 (t, J = 7.32 Hz, 16 H, C_6H_{13}), 0.87 (m, 48 H, C_6H_{13}), 0.78–0.63 (m, 40 H, C_6H_{13}); MS (FAB): m/z 1532.9 (M^+). Anal. Calcd for $C_{116}H_{138}$: C, 90.92; H, 9.08. Found: C, 90.90; H, 8.85.

2.2.6. 1,3,6,8-Tetrakis(7-(9,9-dihexyl-9H-fluoren-2-yl)-9,9-dihexyl-9H-fluoren-2-yl)pyrene (*6*)

Compounds **6** were prepared by similar procedures for preparation of compound **5**, except that 2-bromo-7-(9,9-dihexyl-9*H*-fluoren-2-yl)-9,9-dihexyl-9*H*-fluorene are used. Yield: 92%. Yellow powder. ^1H NMR (400 MHz, acetone-d_6): δ (ppm) 8.25 (s, 4 H, pyrene), 8.19 (s, 2 H, pyrene), 7.9 (d, J = 8.12 Hz, 4 H, C_6H_3), 7.81 (d, J = 7.92 Hz, 4 H, C_6H_3), 7.77 (d, J = 7.96 Hz, 4 H, C_6H_3), 7.73–7.62 (m, 28 H, C_6H_3), 7.73–7.62 (m, 12 H, C_6H_4), 2.15–2.00 (m, 32 H, C_6H_{13}), 1.08–1.06 (m, 96 H, C_6H_{13}), 0.76–0.68 (m, 80 H, C_6H_{13}); MS (FAB): m/z 2863.7 (M^+). Anal. Calcd for $C_{216}H_{266}$: C, 90.63; H, 9.37. Found: C, 90.62; H, 9.12.

2.3. EL device fabrication and characterization of OLEDs

Pre-patterned ITO substrates with an effective individual device area of 3.14 mm^2 were cleaned by using standard procedure. The organic materials were fabricated by thermal evaporation technique, except compound **6**. Two-layered devices using compounds **1**–**5** as the hole-transporting/emitting layer and 1,3,5-tris(*N*-phenylbenzimidizol-2-yl)benzene (TPBI) or tris(8-hydroxy-quinolinato) aluminum (Alq_3) as the electron-transporting layer were fabricated (devices I and II). The devices were prepared by vacuum deposition of 40 nm of the hole-transporting layer, followed by 40 nm of TPBI or Alq_3. Inorganic LiF of 1 nm thick was then deposited as the buffer layer. Aluminum was finally deposited as the cathode (150 nm). In device III, 4,4′-bis[*N*-(1-naphthylphenyl)amino]biphenyl (NPB) was used as the hole-transport layer, and **5** was used as emitting as well as electron-transport layer. In devices IV and V, the films of PVK doped with compound **6** were spin-coated from dichloroethane solution (concentration = 10 mg/mL) at a spin rate of 3000 rpm for 40 s. *I*–*V* curves were measured in a Keithley 2400 Source Meter under the ambient environment. Light intensity was measured with a Newport 1835 Optical Meter. *I*–*V* curve was measured on a Keithley 2000 Source Meter in ambient environment. Light intensity was measured with a Newport 1835 Optical Meter.

2.4. Time-of-flight (TOF) mobility measurement

The samples **5** and **6** for the TOF measurement were prepared by melt deposition using the structure of: glass/Ag (30 nm)/**5** (or **6**) (11–12 μm)/Al (150 nm) with an active area of 2×2 mm^2 as described in previous reports [27,28]. A frequency-tripled Nd:YAG laser (355 nm) with ~10 ns pulse duration was used for pulsed illumination through the semitransparent Ag. Under an applied DC bias, the transient photocurrent as a function of time was recorded with a digital storage oscilloscope. The TOF measurements were typically performed in a 10^{-5}-torr vacuum chamber. Depending on the polarity of the applied bias *V*, selected photogenerated carriers (holes or electrons) are swept across the sample thickness *D* with a transit time t_T, the

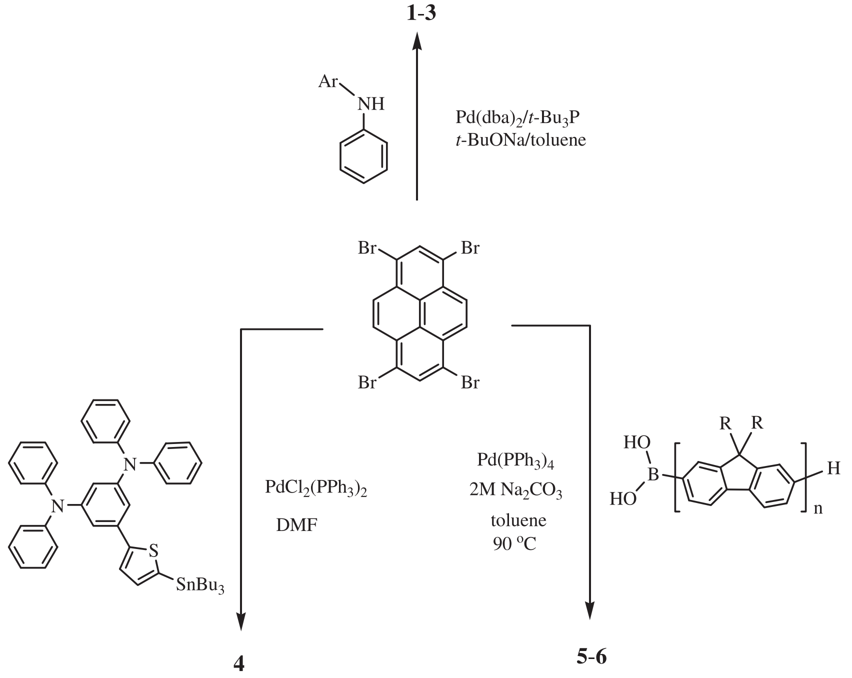

Scheme 1. Synthesis of compounds **1–6**, R = C_6H_{13}.

applied electric field E is then V/D, and the carrier mobility is given by = $D/(t_T \cdot E) = D^2/(V \cdot t_T)$.

3. Results and discussion

3.1. Synthesis

The compounds synthesized in this study are shown in Chart 1. Scheme 1 illustrates synthetic procedures of these compounds. Compounds **1**–**3** were synthesized from 1,3,6,8-tetrabromopyrene and 4.4 equivalents of the corresponding diarylamine following the literature method [29]. Fourfold thienylation of 1,3,6,8-tetrabromopyrene with 4.4 equivalents of stannyl compound, 5-(5-(tributylstannyl)thiophen-2-yl)-1,1,3,3-tetraphenylbenzene-1,3-diamine, using palladium(0)-catalyzed Stille coupling reaction, resulted in formation of **4**. Suzuki coupling reactions of 1,3,6,8-tetrabromopyrene with 5.2 equivalents of the corresponding fluorenylboronic acids yielded **5** and **6** [22]. The new compounds were isolated in moderate to high yields (52–92%). All the compounds were soluble in common solvents (e.g., acetone, CH_2Cl_2) and characterized by ^{1}H NMR, FAB-MS and elemental analysis.

3.2. Thermal properties

The thermal properties of the new compounds were determined by DSC and TGA (Table 1). These compounds have high thermal decomposition temperature (T_d = 414–522 °C). All the compounds exhibited melting isotherms during the first heating cycle, but rapid cooling of the melt led to the formation of a glassy state which persisted in the subsequent heating cycles. No glass transition was noticed for **1** and **5**, while the glass transition temperatures (T_g) of **2**–**4** are higher than 160 °C. Compound **6** has a much lower T_g value, which is attributed to the presence of the flexible alkyl chains of the fluorenyl segments.

3.3. Photophysical properties

The absorption and luminescence spectral data of the compounds are presented in Table 1. Representative absorption and emission spectra in solution are shown in Fig. 1. The bands at 400–469 nm are ascribed to the $\pi \rightarrow \pi^*$ transition of the pyrene moiety. The longer wavelength absorption in **1**–**3** than in **5**–**6** can be attributed the mixing of $\pi \rightarrow \pi^*$ transition with $n \rightarrow \pi^*$ transition from the nitrogen lone pair to the pyrene moiety. Compound **4**

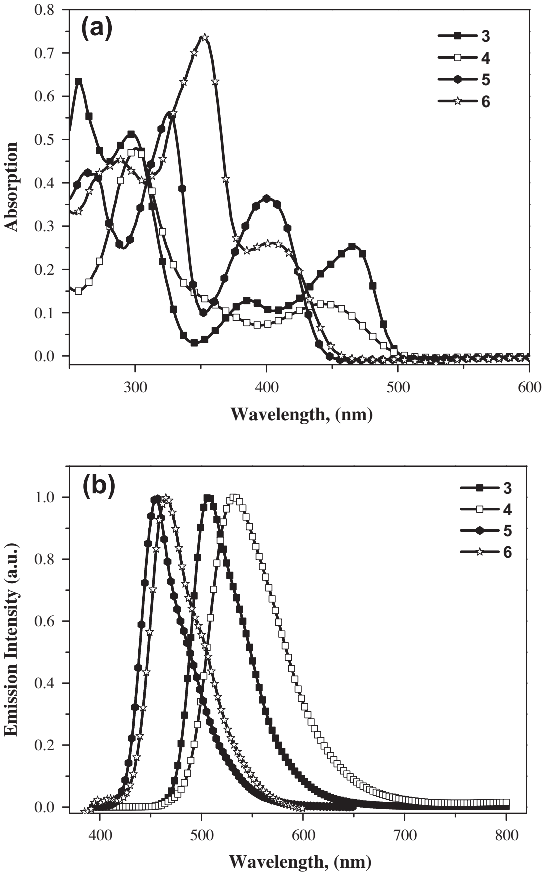

Fig. 1. The absorption (a) and emission (b) spectra of the compounds in CH_2Cl_2.

Table 1
Physical data for compounds **1**–**6**.

	$T_g/T_c/T_m$ (°C)[a]	T_d (°C)[a]	λ_{max} (nm)[b]	λ_{em} (nm) sol[b]/film[c]	Φ_f (%) sol[d]/solid[e]	E_{ox} ($\triangle E_p$) (mV)[f]	HOMO/LUMO (eV)[g]
1	NA/287/367	414	257, 299, 383, 463	500/524	69/57	137 (163), 1187 (i)	−4.94/−2.50
2	172/261/342	440	257, 300, 367, 466	500/525	62/55	112 (160), 1197 (i)	−4.91/−2.49
3	162/214/298	426	263, 302, 388, 462	507/526	74/60	95 (158), 1217 (i)	−4.90/−2.43
4	167/266/372	522	301, 351, 443	532/533	16/13	617 (i)	−5.41/−3.00
5	NA/164/186	409	262, 326, 401	455/485	83/68	847 (163), 1177 (174)	−5.65/−2.91
6	87/NA/212	414	289, 351, 405	465/493	79/62	886 (143), 1200 (169)	−5.69/−3.02

[a] T_g, glass transition temperature; T_c, crystallization temperature; T_m, melting point; T_d, thermal decomposition temperature; NA, not detected.

[b] λ_{max}, absorption maximum; measured in CH_2Cl_2 solution; λ_{em}, emission maximum; measured in CH_2Cl_2 solution.

[c] λ_{em}, emission maximum; measured in the film cast on glass substance.

[d] Quantum yield (Φ_f) was measured relative to Coumarin 1 (99% in ethyl acetate) [25]. Corrections due to change in solvent refractive indices were applied.

[e] Quantum yield (Φ_f) was measured in solid state by integration sphere.

[f] All E_{ox} data are reported relative to ferrocene which has an E_{ox} at 223 mV relative to Ag/Ag$^+$ and the anodic peak–cathodic peak separation ($\triangle E_p$) is 75 mV. The concentration of the compound was 5×10^{-3} M and the scan rate was 100 mV s^{-1}; i, irreversible.

[g] LUMO levels were derived via eq. E_g = HOMO–LUMO.

exhibits a blue shift of absorption compared with **1**–**3**, which may be due to the *meta*-substitution of the peripheral diphenylamines, leading to less efficient interaction between the amines and the pyrene core. In the solution, the emission colors range from blue (**5**–**6**, 455–465 nm) to green (**1**–**4**, 500–532 nm) (Fig. 1b). The photoluminescence spectra in the film states were also measured. The film emission spectra (Fig. S1, Supporting Information) were broadened only slightly compared with the solution spectra, indicating no significant dye aggregation. All the compounds except **4** are strongly emissive in dichloromethane, with the PL quantum yields (Φ_f) ranging from 16% to 83%. Insufficient orbital overlap between HOMO and LUMO in the $S_0 \rightarrow S_1$ transition likely causes lower solution quantum yield of **4** as the arylamines reside at *meta*-disposition relative to the conjugated spacer. The large difference in MO population between the S_0 and S_1 states also leads to large Stokes shift in **4** than the others. The full widths at half maximum (FWHM) of the emission spectra in general are very small (<60 nm) except for **4** (90 nm), which is beneficial to saturated monochromatic emission.

3.4. Electrochemical properties

The electrochemical data of all compounds are listed in Table 1. Representative cyclic voltammograms of selected compounds are shown in Fig. S2 (Supporting Information). 1,3,6,8-Tetrakis-(dimethylamino)pyrene was reported to exhibits two reversible redox waves due to the oxidation of the amine [30]. However, the oxidation of arylamines (**1**–**3**) was observed as a quasi-reversible wave at slightly higher potential than previous report. The oxidation potential of the compounds increases in the order of **3** < **2** < **1**, in accordance with the decreasing electron-donating ability of the substituents. The oxidation of the arylamines in **4** is irreversible and at higher potential than that in **1**–**3**. This is in accordance with our previous observation: pyrenylamine has a lower oxidation potential than phenylamine [9]. Compounds **5** and **6** are oxidized at a much higher potential than **1**–**4**, due to the absence of the amino units. In contrast to **1**–**4**, two quasi-reversible oxidation processes were detected for **5** and **6**.

3.5. Theoretical calculation

Density functional calculations at B3LYP/6-31G* level were carried out on the pyrene compounds. Fig. 2 shows the frontier orbitals for the representative compounds **3**, **4** and **5**. The HOMOs of **1**–**3** are distributed from pyrene to the arylamine, whereas their LUMOs mainly localized on the pyrene entity (Fig. S3, Supporting Information). For compound **4**–**6**, both HOMO and LUMO for each compound populate at pyrene and four aryl substituents. There is only little MO population on the diphenylamino groups of compound **4**, showing the interruption of electronic communication between pyrene and diphenylamine by meta-conjugation. The calculated energy gap (E_g) increased

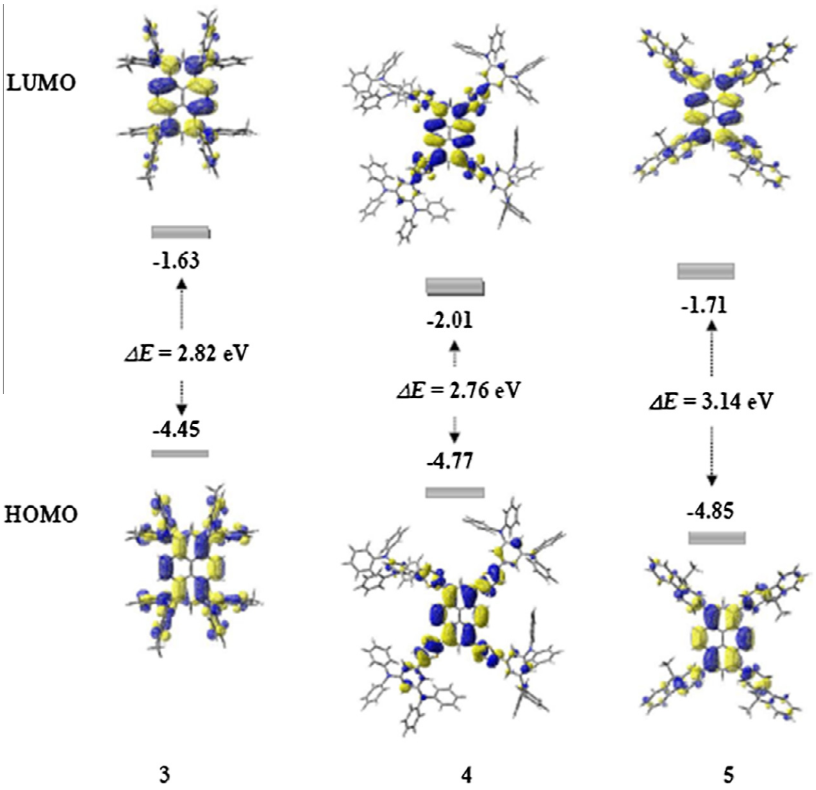

Fig. 2. Calculated molecular orbital and energy levels of model compounds of **3**, **4** and **5**.

Table 2
Performance characteristics of the devices.

Devices	**1**[a]	**2**[a]	**3**[a]	**4**[a]	**5**[b]	**6**[c]
V_{on} (V)	2.6; 2.4	2.5; 2.3	2.1; 2.1	4.2; 3.8	3.3; 3.0; 4.2	5.6; 4.2
L_{max} (cd/m^2)	13,696; 14,313	22,212; 23,329	8784; 11,290	6765; 18,351	10,035; 11,088; 17,118	3249; 9755
$\eta_{ex,max}$ (%)	1.4; 1.7	1.1; 1.3	2.0; 1.1	0.59; 0.62	2.7; 1.0; 3.2	0.34; 3.2
$\eta_{c,max}$ (cd/A)	4.4; 5.5	3.7; 4.0	6.2; 3.6	1.6; 1.8	4.3; 3.1; 5.0	0.42; 4.5
$\eta_{p,max}$ (lm/W)	4.6; 5.8	3.8; 4.2	6.5; 3.7	1.3; 1.4	2.7; 2.5; 2.1	0.11; 1.6
λ_{max} (nm)	502; 504	508; 508	504; 504	532; 526	468; 516; 470	472; 468
FWHM (nm)	60; 66	52; 52	46; 48	126; 94	62; 104; 64	54; 54
CIE (x, y)	0.28, 0.58; 0.28, 0.59	0.24, 0.63; 0.25, 0.63	0.19, 0.62; 0.20, 0.62	0.39, 0.52; 0.33, 0.56	0.16, 0.22; 0.27; 0.49; 0.14, 0.22	0.12, 0.17; 0.15, 0.19
V[d]	5.5; 6.3	4.8; 6.0	7.0; 7.0	8.5; 8.2	6.5; 7.1; 11	13; 14.5
L (cd/m^2) [d]	2730; 2797	2829; 2625	970; 1945	2168; 194	3300; 2870; 4165	420; 2679
η_{ex} (%) [d]	0.88; 0.89	0.87; 0.80	0.71; 0.64	0.36; 0.63	2.2; 0.97; 2.7	0.34; 2.0
η_c (cd/A) [d]	2.7; 2.8	2.8; 2.6	2.2; 2.0	0.97; 2.0	3.3; 2.9; 4.2	0.42; 2.7
η_p (lm/W) [d]	1.6; 1.4	1.8; 1.4	0.98; 0.90	0.36; 0.72	1.6; 1.3; 1.2	0.10; 0.58

[a] The measured values are given in order of the devices I and II.

[b] The measured values are given in order of the devices I–III.

[c] The measured values are in order of the devices IV and V.

[d] The measured values were taken at a current density of 100 mA. L_{max}, maximum luminance; $\eta_{ex,max}$, maximum external quantum efficiency; $\eta_{c,max}$, maximum current efficiency; $\eta_{p,max}$, maximum power efficiency; FWHM, full width at half maximum; V, voltage; L, luminance; η_{ex}, external quantum efficiency; η_c, current efficiency; η_p, power efficiency.

from *ca.* 2.8 eV (**1**–**4**) to 3.14 eV (**5**) with the absence of the strong amino donor. These values are in good agreement with those estimated from the optical absorption edge (Table 1). It is clear that the E_g of pyrene derivatives can be adjusted via substituted aryl groups, indicating tunable emission wavelength of the pyrene chromophores.

3.6. Electroluminescent properties

The HOMO energy levels of the compounds were calculated from cyclic voltammetry reference to ferrocene (4.8 eV) [31]. These data together with the absorption spectra were then used to obtain the LUMO energy levels (Table 1). Considering the energy levels (Fig. 7) and carrier-transporting characteristics of these compounds, two-layered devices having three different structures were fabricated: (I) ITO/**1** (or **2**–**5**) (40 nm)/TPBI (40 nm)/LiF (1 nm)/Al (150 nm); (II) ITO/**1** (or **2**–**5**) (40 nm)/Alq$_3$ (40 nm)/LiF (1 nm)/Al (150 nm); (III) ITO/NPB (40 nm)/**5** (40 nm)/LiF (1 nm)/Al (150 nm). Compounds **1**–**5** were used as the emitting as well as hole-transporting layer in both devices I and II. TPBI and Alq$_3$ were used as electron-transporting layer in the devices I and II, respectively. In viewing that **5** exhibits good electron transport ability (vide infra), device III consisting of NPB as the hole-transporting layer, and **5** as the emitting as well as electron-transporting layer was also fabricated. The performances of various devices are summarized in Table 2. *I*–*V*–*L* characteristics for the devices I–III are shown in Figs. 3 and 4, and the EL spectra are shown in Fig. 5. For **1**–**3**, the EL spectra of the devices I and II bear resemblance to the film spectra of EML, indicating the excitons are effectively confined in the EML. For **4**, the EL spectrum of the device II resembles the film spectra of **4**. In comparison, the EL spectrum of the device I is broader than the film spectra of **4** at the longer wavelength portion, even though the excitons are mainly confined in the EML. The observation of the broad emission band is attributed to exciplex formation since similar spectra was also observed in the blend film

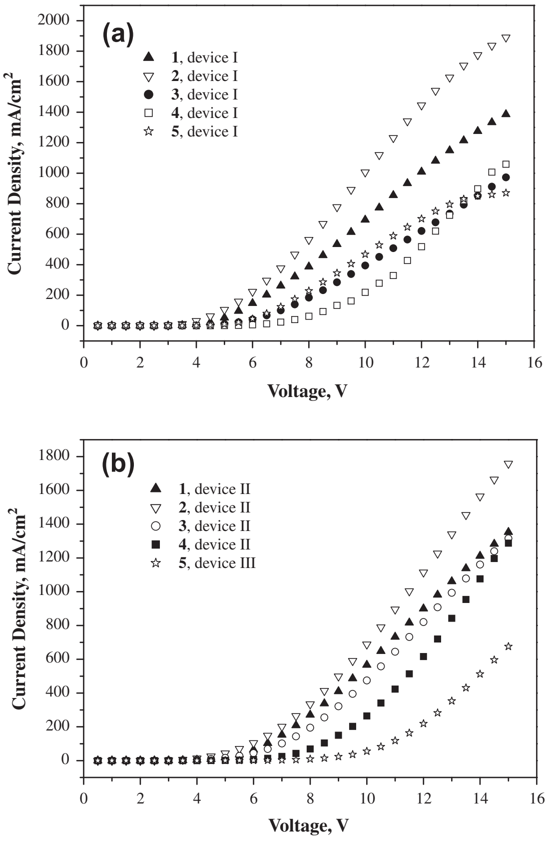

Fig. 3. Current density–voltage characteristics of the devices. (a) Device I. (b) Devices II and III.

of **4** and TPBI. Efficiencies (Table 2) of both devices I and II for **1**–**4** drop significantly as the applied voltage (or current density) increases.

Both devices I and III of **5** emit blue light characteristic of **5**, confirming that **5** is capable of transporting both electrons and holes (which will be further discussed in next section). Both devices have good performance parameters (I: L, 3300 cd/m^2; η_{ex}, 2.2%; η_c, 3.3 cd/A; η_p, 1.6 lm/W and III: L, 4165 cd/m^2; η_{ex}, 2.7%; η_c, 4.2 cd/A; η_p, 1.2 lm/W at a current density of 100 mA/cm^2). Moreover, the non-optimized device III also appears to have reasonably stable external quantum efficiency and current efficiency at high current levels (Fig. 6). It is worth noting that the two devices have very narrow full widths at half maximum (FWHM ~ 60 nm) in EL spectra, which is required for saturated monochromatic emission. In contrast to the devices I and III, the device II of **5** emitted green light characteristic of Alq$_3$. Obviously the smaller energy barrier between the HOMO of **5** and Alq$_3$ (6.0 eV) allows passage of holes form **5** to Alq$_3$. In comparison, TPBI acts as an effective hole blocker due to its lower HOMO level (6.2 eV). Consequently, excitons are effectively confined inside the layer of **5**.

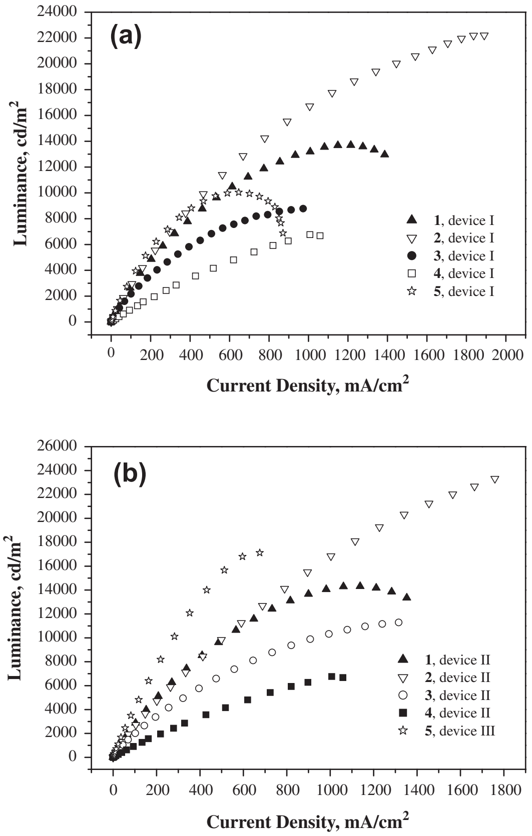

Fig. 4. Luminescence–current density characteristics of the devices. (a) Device I. (b) Devices II and III.

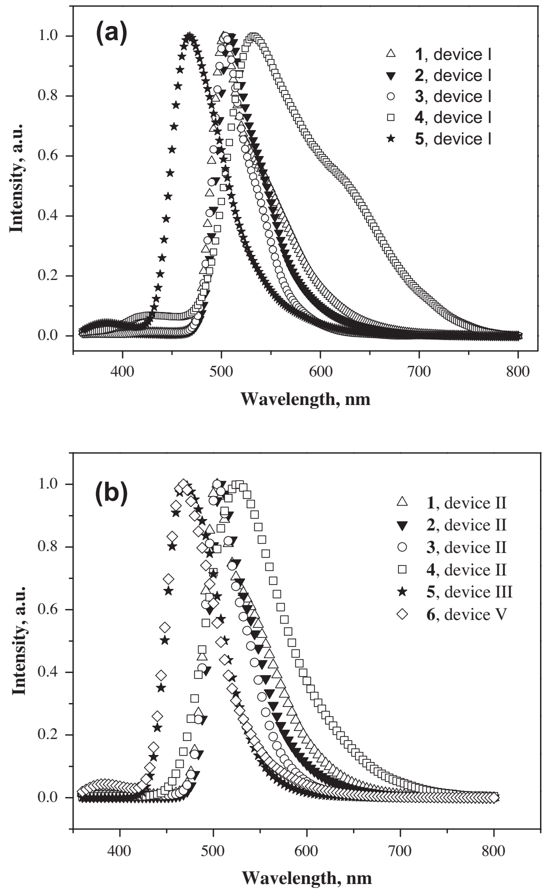

Fig. 5. EL spectra of the devices. (a) Device I. (b) Devices II, III and V.

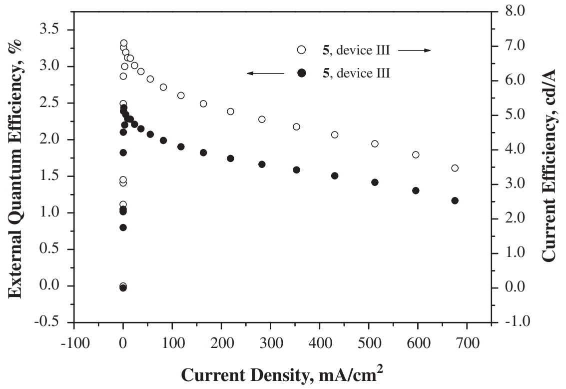

Fig. 6. Current efficiency and external quantum efficiency versus current density for device III of **5**.

Due to the low volatility of **6** (and thus difficulty in preparing films via vacuum deposition), device IV having the structure of ITO/PEDOT:PSS (70 nm)/PVK + **6** (30 wt.%) (60 nm)/LiF (1 nm)/Al (150 nm) (PEDOT:PSS = polyethylenedioxythiophene:polystyrene-sulfonate; PVK = poly(vinylcarbazole)), was fabricated via the spin-coating technique. Blue light (λ_{em} = 472 nm; (x, y) = (0.12, 0.17); FWHM = 54 nm) characteristic of **6** was observed in this device. However, the performance (L_{max}, 3249 cd/m^2; $\eta_{ex,max}$, 0.34%; $\eta_{c,max}$, 0.42 cd/A; $\eta_{p,max}$ 0.11 lm/W) is only mediocre. If TPBI is deposited on the top of the PVK/**6** blend layer, i.e., ITO/PEDOT:PSS (70 nm)/PVK + **6** (30 wt.%) (60 nm)/TPBI (40 nm)/LiF (1 nm)/Al (150 nm) (device V),

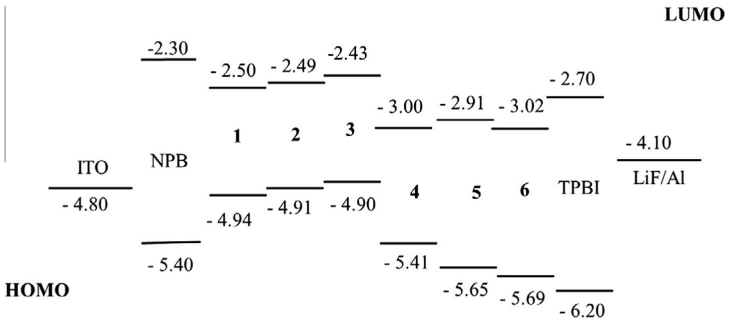

Fig. 7. Energy level diagram of the materials used for the fabrication of devices.

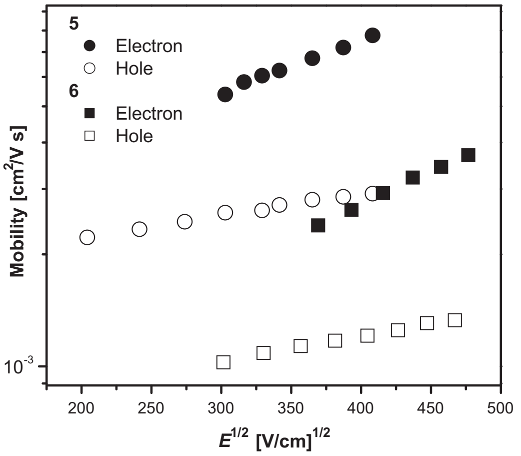

Fig. 8. Electron and hole mobilities versus $E^{1/2}$ for **5** and **6**.

the performance increases significantly: (L_{max}, 9755 cd/m^2; $\eta_{ex,max}$, 3.2%; $\eta_{c,max}$, 4.6 cd/A; $\eta_{p,max}$ 1.6 lm/W). If TPBI was replaced with Alq$_3$, both **6** and Alq$_3$ made significant contributions to the light emission.

3.7. Charge-transport properties

Since **5** can be used as an electron- as well as a hole-transporting layer and similar structural motifs are present in **5** and **6**, carrier-transport properties of both were investigated by the TOF transient photocurrent technique at room temperature. Both **5** and **6** reveal non-dispersive hole-transport and dispersive electron-transport characteristics. The carrier transit time t_T needed for determining carrier mobilities was evaluated from the intersection point of two asymptotes in the double logarithmic representation (insets of Fig. S4, Supporting Information). The carrier mobilities of **5** and **6** thus determined are shown in Fig. 8 as a function of the electric field E. The field dependence of carrier mobilities of **5** and **6** follows the nearly universal Poole–Frenkel relationship: $\mu \propto \exp(\beta E^{1/2})$, where β is the Poole–Frenkel factor [32]. Electron mobilities of **5** and **6** are in the range of 10^{-3}–10^{-2} cm^2/V s, which are nearly two-orders higher than those of the typical electron-transport material Alq$_3$ (~10^{-5} cm^2/V s) [33]. Some ter(9,10-diarylfluorene) derivatives were also reported to have rather high electron mobilities (>10^{-3} cm^2/V s) in amorphous solid states [27]. The presence of oligofluorene moiety in compound **5** and **6** may prevent of the formation of deep electron trapping due to oxygen, which affect the carrier transport in molecule.

Interestingly, compound **5** and **6** exhibit ambipolar transporting properties though both do not contain strongly electron-deficient moieties in the molecular skeleton [34]. The hole mobilities of **5** and **6** also appear to be very high, (>10^{-3} cm^2/V s), and are higher than those of the typical hole-transport material NPB [35].

4. Conclusions

We have synthesized star-shaped molecules based on tetra-substituted pyrene. They are highly thermally stable and exhibit high glass transition temperatures. Compounds containing peripheral arylamines can be used as hole-transporting and green-emitting materials for electroluminescent devices. The compounds with peripheral fluorenes are blue-emitting and exhibit bipolar carrier transport characteristics. Both electron and hole mobilities measured by TOF method surpass 10^{-3} cm^2/V s. Two-layered devices using the blue-emitting compound as the hole-transporting and the emitting layer or as the electron-transporting and the emitting layer exhibited good performances. Most devices in this study have relatively narrow FWHMs (~60 nm).

Acknowledgements

This work was supported by the TIGP program (Academia Sinica), National Science Council, Academia Sinica Institute of Chemistry (AC), National Taiwan University, and the Chinese Culture University, the Instrumental Center of Institute of Chemistry (AC).

Appendix A. Supplementary material

Supplementary data associated with this article can be found, in the online version, at http://dx.doi.org/10.1016/j.orgel.2014.06.003.

References

[1] C.W. Tang, S.A. Vanslyke, Organic electroluminescent diodes, Appl. Phys. Lett. 51 (1987) 913–915.

[2] J.H. Burroughes, D.D.C. Bradley, A.R. Brown, R.N. Marks, K. Mackay, R.H. Friend, P.L. Burns, A.B. Holmes, Light-emitting-diodes based on conjugated polymers, Nature 347 (1990) 539–541.

[3] Y. Shirota, Organic materials for electronic and optoelectronic devices, J. Mater. Chem. 10 (2000) 1–25.

[4] P. Strohriegl, J.V. Grazulevicius, Charge-transporting molecular glasses, Adv. Mater. 14 (2002) 1439–1442.

[5] Y. Shirota, Photo- and electroactive amorphous molecular materials – molecular design, syntheses, reactions, properties, and applications, J. Mater. Chem. 15 (2005) 75–93.

[6] Y. Shirota, H. Kageyama, Charge carrier transporting molecular materials and their applications in devices, Chem. Rev. 107 (2007) 953–1010.

[7] P. Kundu, K.R.J. Thomas, J.T. Lin, Y.T. Tao, C.H. Chien, High-Tg carbazole derivatives as blue-emitting hole-transporting materials for electroluminescent devices, Adv. Funct. Mater. 13 (2003) 445–452.

[8] M. Velusamy, K.R.J. Thomas, J.T. Lin, Y.S. Wen, Benzo[1,2,5]selenadiazole bridged amines: electro-optical properties, Tetrahedron Lett. 46 (2005) 7647–7651.

[9] K.R.J. Thomas, J.T. Lin, Y.T. Tao, C.W. Ko, Light-emitting carbazole derivatives: potential electroluminescent materials, J. Am. Chem. Soc. 123 (2001) 9404–9411.

[10] J.N. Moorthy, P. Natarajan, P. Venkatakrishnan, D.F. Huang, T.J. Chow, Steric inhibition of pi-stacking: 1,3,6,8-tetraarylpyrenes as efficient blue emitters in organic light emitting diodes (OLEDs), Org. Lett. 9 (2007) 5215–5218.

[11] S.L. Tao, Y.C. Zhou, C.S. Lee, X.H. Zhang, S.T. Lee, High-efficiency nondoped deep-blue-emitting organic electroluminescent device, Chem. Mater. 22 (2010) 2138–2141.

[12] Z.Q. Wang, C. Xu, W.Z. Wang, W.J. Fu, L.B. Niu, B.M. Ji, Highly efficient undoped deep-blue electroluminescent device based on a novel pyrene derivative, Solid State Electron. 54 (2010) 524–526.

[13] S.L. Lai, Q.X. Tong, M.Y. Chan, T.W. Ng, M.F. Lo, S.T. Lee, C.S. Lee, Distinct electroluminescent properties of triphenylamine derivatives in blue organic light-emitting devices, J. Mater. Chem. 21 (2011) 1206–1211.

[14] V. de Halleux, J.P. Calbert, P. Brocorens, J. Cornil, J.P. Declercq, J.L. Bredas, Y. Geerts, 1,3,6,8-Tetraphenylpyrene derivatives: towards fluorescent liquid-crystalline columns?, Adv Funct. Mater. 14 (2004) 649–659.

[15] O. Thiebaut, H. Bock, E. Grelet, Face-on oriented bilayer of two discotic columnar liquid crystals for organic donor-acceptor heterojunction, J. Am. Chem. Soc. 132 (2010) 6886–6888.

[16] H.J. Zhang, Y. Wang, K.Z. Shao, Y.Q. Liu, S.Y. Chen, W.F. Qiu, X.B. Sun, T. Qi, Y.Q. Ma, G. Yu, Z.M. Su, D.B. Zhu, Novel butterfly pyrene-based organic semiconductors for field effect transistors, Chem. Commun. (2006) 755–757.

[17] L. Zophel, D. Beckmann, V. Enkelmann, D. Chercka, R. Rieger, K. Mullen, Asymmetric pyrene derivatives for organic field-effect transistors, Chem. Commun. 47 (2011) 6960–6962.

[18] B. Valeur, I. Leray, Design principles of fluorescent molecular sensors for cation recognition, Coord. Chem. Rev. 205 (2000) 3–40.

[19] T.M. Figueira-Duarte, K. Mullen, Pyrene-based materials for organic electronics, Chem. Rev. 111 (2011) 7260–7314.

[20] X.W. Xiao, W. Xu, D.Q. Zhang, H. Xu, L. Liu, D.B. Zhu, Novel redox-fluorescence switch based on a triad containing tetrathiafulvalene and pyrene units with tunable monomer and excimer emissions, New J. Chem. 29 (2005) 1291–1294.

[21] I. Prieto, J. Teetsov, M.A. Fox, D.A.V. Bout, A.J. Bard, A study of excimer emission in solutions of poly(9,9-dioctylfluorene) using electrogenerated chemiluminescence, J. Phys. Chem. A 105 (2001) 520–523.

[22] F. Liu, W.Y. Lai, C. Tang, H.B. Wu, Q.Q. Chen, B. Peng, W. Wei, W. Huang, Y. Cao, Synthesis and characterization of pyrene-centered Starburst oligofluorenes, Macromol. Rapid Commun. 29 (2008) 659–664.

[23] P. Sonar, M.S. Soh, Y.H. Cheng, J.T. Henssler, A. Sellinger, 1,3,6,8-Tetrasubstituted pyrenes: solution-processable materials for application in organic electronics, Org. Lett. 12 (2010) 3292–3295.

[24] K.R.J. Thomas, N. Kapoor, M.N.K.P. Bolisetty, J.H. Jou, Y.L. Chen, Y.C. Jou, Pyrene–fluorene hybrids containing acetylene linkage as color-tunable emitting materials for organic light-emitting diodes, J. Org. Chem. 77 (2012) 3921–3932.

[25] S. Bernhardt, M. Kastler, V. Enkelmann, M. Baumgarten, K. Mullen, Pyrene as chromophore and electrophore: encapsulation in a rigid polyphenylene shell, Chem.-Eur. J. 12 (2006) 6117–6128.

[26] C.C. Wu, T.L. Liu, W.Y. Hung, Y.T. Lin, K.T. Wong, R.T. Chen, Y.M. Chen, Y.Y. Chien, Unusual nondispersive ambipolar carrier transport and high electron mobility in amorphous ter(9,9-diarylfluorene)s, J. Am. Chem. Soc. 125 (2003) 3710–3711.

[27] L.Y. Chen, W.Y. Hung, Y.T. Lin, C.C. Wu, T.C. Chao, T.H. Hung, K.T. Wong, Enhancement of bipolar carrier transport in oligofluorene films through alignment in the liquid-crystalline phase, Appl. Phys. Lett. 87 (2005) 112103–112103-3.

[28] J.Y. Hu, M. Era, M.R.J. Elsegood, T. Yamato, Synthesis and photophysical properties of pyrene-based light-emitting monomers: highly pure-blue-fluorescent, cruciform-shaped architectures, Eur. J. Org. Chem. (2010) 72–79.

[29] N. Ueda, Y. Sakata, S. Misumi, Synthesis of 1,3,6,8-tetrakis(dimethylamino)pyrene having low oxidation potential, B. Chem. Soc. Jpn. 59 (1986) 3289–3290.

[30] Y.J. Xing, X.J. Xu, P. Zhang, W.J. Tian, G. Yu, P. Lu, Y.Q. Liu, D.B. Zhu, Carbazole–pyrene-based organic emitters for electroluminescent device, Chem. Phys. Lett. 408 (2005) 169–173.

[31] J. Pommerehne, H. Vestweber, W. Guss, R.F. Mahrt, H. Bassler, M. Porsch, J. Daub, Efficient 2-layer leds on a polymer blend basis, Adv. Mater. 7 (1995) 551–554.

[32] H. Bassler, Hopping conduction in polymers, Int. J. Mod. Phys. B 8 (1994) 847–854.

[33] A.P. Kulkarni, C.J. Tonzola, A. Babel, S.A. Jenekhe, Electron transport materials for organic light-emitting diodes, Chem. Mater. 16 (2004) 4556–4573.

[34] M.J. Sienkowska, H. Monobe, P. Kaszynski, Y. Shimizu, Photoconductivity of liquid crystalline derivatives of pyrene and carbazole, J. Mater. Chem. 17 (2007) 1392–1398.

[35] Y.Q. Li, M.K. Fung, Z.Y. Xie, S.T. Lee, L.S. Hung, J.M. Shi, An efficient pure blue organic light-emitting device with low driving voltages, Adv. Mater. 14 (2002) 1317–1321.